

## EVALUATION AND ASSESSMENT OF ARCTANGENT-BASED POST-GLACIAL LAND UPLIFT MODEL

*Jari Pohjola<sup>1</sup>, Tarmo Lipping<sup>1</sup>, Jari Turunen<sup>1</sup>, and Ari T.K. Ikonen<sup>2</sup>*

1. Tampere University of Technology, Pori, Department of Signal Processing, Pori, Finland; {[jari.pohjola](mailto:jari.pohjola@tut.fi) / [tarmo.lipping](mailto:tarmo.lipping@tut.fi) / [jari.j.turunen](mailto:jari.j.turunen@tut.fi)}@tut.fi
2. Posiva Oy, Eurajoki, Finland; [ari.ikonen@posiva.fi](mailto:ari.ikonen@posiva.fi)

### ABSTRACT

This paper describes a new method for improved estimation of the parameters of a semi-empirical land uplift model of Fennoscandia, introduced by Tore Pässe in 2001. The behaviour and the basis of the land uplift model parameters are also evaluated. The ongoing land uplift in the Baltic Sea region is due to the rebound of glacial stress caused by the most recent ice age 115,000-10,000 years before present (BP). The improved methodology for the land uplift model parameter estimation presented in this study is based on regional variations in bedrock properties and download. The parameters are computed using ancient shore level positions and information about the pre-historic population in Finland. Because of the uncertainties and inaccuracies in the radiocarbon dating and the shore level estimations, Monte Carlo simulation was employed for the estimation of the parameter distributions. The resulting parameter estimates indicate the possibility of local variations in land uplift in Finland.

### INTRODUCTION

Post-glacial crustal rebound (Figure 1) is a phenomenon affecting, for example, the nuclear waste disposal sites in Fennoscandia. Sustainability of the nuclear waste disposal facilities for over several thousands of years and beyond must be evaluated and therefore plausible crustal rebound models need to be developed. In case of a containment failure scenario, a broken nuclear disposal canister will emit radionuclides to the environment. Surface water bodies are the major transport channels for radionuclides in this kind of scenario. Land uplift will have an impact on river flow directions and thus it is very important to estimate the location and formation of water bodies in order to analyse the cumulative radionuclide dose for people and biota in the future. Surface water body estimation is best accomplished by combining the crustal rebound model with the present digital elevation model (incl. the seabed) as well as hydrological and biosphere modelling to derive scenarios for the future development of the landscape.

In this paper, we concentrate on the future behaviour of the crustal rebound process, however, this will be just one of the three steps in our landscape modelling effort. As the first step we created the digital elevation model of a test area surrounding the Olkiluoto nuclear waste repository site in Western Finland using airborne lidar data (1) as well as satellite altimetry data (2) and sonar data for seabed mapping. As the third step we will combine the results of digital elevation, crustal rebound and biosphere modelling using a custom-made GIS toolbox to predict the future formation of surface water bodies due to land uplift.

Two different approaches can be taken to model the post-glacial crustal rebound: The model may either be based on the detailed geological processes causing the crustal rebound (3,4) or, alternatively, simple curve-fitting techniques may be applied. It is commonly accepted that the geological processes are not well enough understood or are too complex to yield a feasible larger-scale crustal rebound model. For crustal rebound modelling by curve-fitting, a suitable mathematical function must be selected first and the parameters of the function must be determined based on the data available on the land uplift and coastline displacement as it has happened in the past. The most commonly used method for modelling crustal rebound in Fennoscandia employs an arctangent-based function (5). The parameters of the function have been given physical meaning as follows:

- 1) deformation of the crust due to the ice load
- 2) crustal inertia
- 3) timing of the ice sheet recession.

However, the physical meaning of the parameters is more or less explanatory and does not rely on any physical model but rather on the behaviour of the chosen function by its attributes.

In this paper, the crustal rebound model is refined by incorporating archaeological data to fine-tune the model parameters using a Monte Carlo approach. The model parameters were determined by finding the local minima of the error between the land uplift as described by the model and by the available data points. After facing several discrepancies we concentrated on analysing the behaviour of the error surface. It became obvious that with respect to the 'ice load parameter', the error surface tends to be flat missing a single minimum. This means that there is no unambiguous solution for a certain parameter combination. In addition, the 'crustal inertia parameter' does not correlate properly with the latest lithosphere data. For the analysis of shore level displacement, also data on the eustatic sea level is needed. The eustatic model employed in (5) is generic and does not take into account all the eustatic oscillations of the Baltic Sea during the last 10,000 years.

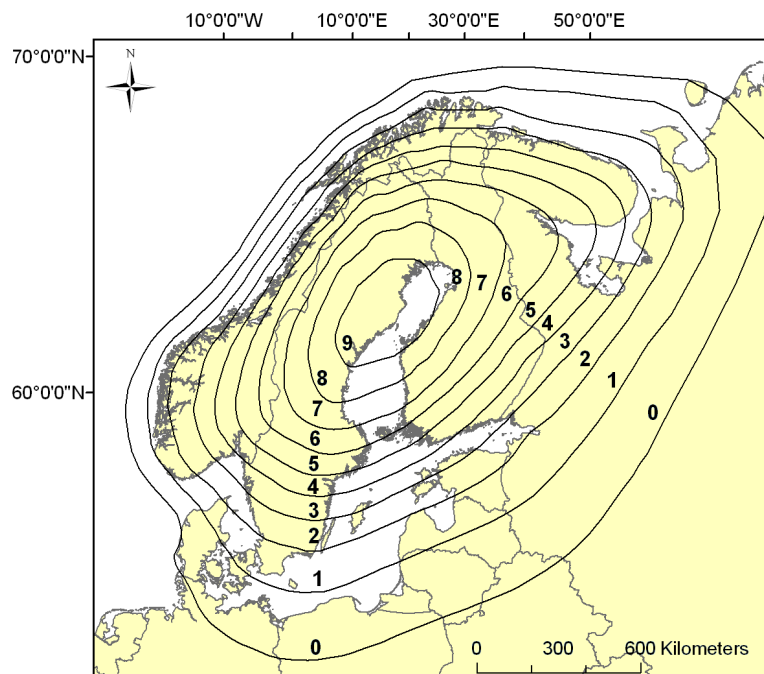


Figure 1: Absolute annual land uplift in millimetres in Fennoscandia. The figure has been modified from (6).

The aim of this paper is to improve the practical arctangent-based crustal rebound model and to discuss the drawbacks and contradictions involved in the model by analysing the behaviour of the model error with respect to the available data.

**METHODS**

**Påsse’s uplift model**

In Påsse’s model (5) the vertical shore level displacement is expressed as:

$$S = U - E \tag{1}$$

$$U = U_s + U_f \tag{2}$$

where  $S$  is the shore level displacement,  $U$  is the total glacio-isostatic uplift,  $U_s$  and  $U_f$  are the slow and fast components of the glacio-isostatic uplift, respectively, and  $E$  is the eustatic sea level rise (all in metres). The components of the model are illustrated in Figure 2 (left-hand side). In the fig-

ure, the altitudes corresponding to the components of the model are shown instead of the rate of change. This can be done provided that a certain reference level is chosen. The figure follows the convention used in (5) of setting the reference point at the altitude of the sea level in AD 1950, common practice also in carbon dating (e.g. before/after 'present', BP/AP).

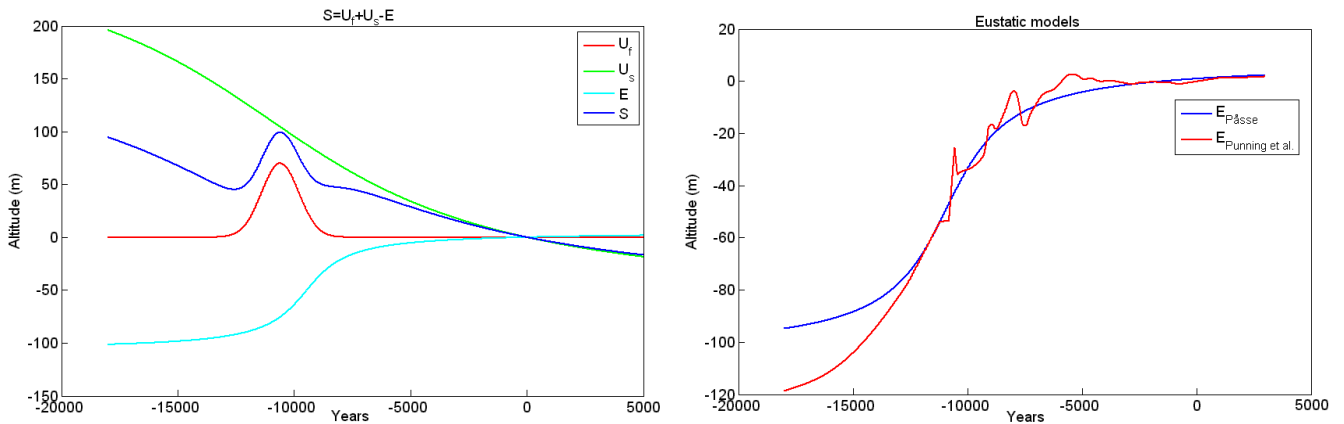


Figure 2: Left-hand side: An example of shore level displacement, slow and fast uplift and eustatic sea level rise following an illustration in (5). Right-hand side: Sea and lake level estimates. The blue curve is the eustatic rise according to (5). The red curve is the alternative eustatic model obtained by combining the data from (7,8,9,10,11).

**Estimation of eustatic sea level rise**

The eustatic model used by Pässe in Eq. (1) is expressed as (5):

$$E = \frac{2}{\pi} \cdot 56 \cdot \left[ \arctan\left(\frac{9500}{1350}\right) - \arctan\left(\frac{9500 - t}{1350}\right) \right] \tag{3}$$

Pässe derived this function using an iterative procedure, where the difference between the hypothetical uplift curves and empirical shore level curves was calculated (5). In our study, an alternative eustatic model is used in parallel with the eustatic model by Pässe. The alternative model is based on water level data from several sources. The main component of the model in the time range of the past 10,000 years is the eustatic curve presented in (7), where the water level changes in the Baltic Sea area have been described. Radiocarbon-dated coral data collected in (8,9,10) and information about the past lake phases in the Baltic Sea area (11) are used to extend the model beyond 10,000 BP.

It is well known that there were two periods during the past 15,000 years when the Baltic Sea actually formed a lake being separated from the oceans. These periods are referred to as lake phases: the Baltic Ice Lake (12,600 - 10,300 BP) and the Ancylus Lake (9,500 - 9,000 BP) (11). Pässe discussed the effects of the lake phases on the parameters of the shore level displacement model and concluded that the evidence is insufficient and that the influence of these lakes might be negligible in long-term studies (5). This is true, if only the future land uplift is of interest and the parameter values are fully known. However, in order to use the observations from the lake periods in determining the model parameter values necessary also for the prospective simulations, a correction to the eustatic curve is needed. The eustasy in the Baltic Sea has a correlation with the eustasy in the North Sea (12). The level of the Baltic Sea follows the level of the North Sea that is 20 cm (long-term average) higher than the global mean sea level (13). The narrow straits connecting the Baltic Sea to the Atlantic referred to as The Danish Straits, and the long-term water balance have also influence on the Baltic Sea level (14). Depending on the resolution of the land uplift model, these effects can be considered not significant.

In our study the estimates of the duration of the lake phases and the altitude of the water level in the lakes as described in (11) were combined with the water level oscillations in the Baltic Sea area as described in (7) and the coral data from (8,9,10) using polynomial approximation to yield an alternative eustatic model. In Figure 2 (right-hand side), both eustatic models, the one used in (5)

and the alternative model, are presented. We refer to the alternative model as Punning et al.'s eu-static model. It can be seen from the figure that during the lake phases the water level remained significantly higher compared to the global sea level until the connection opened again.

**Parameters describing the slow uplift**

In this study, the focus of the parameter adjustment was on the slow land uplift  $U_s$ , because the effect of the fast uplift  $U_f$  was evident only shortly after the melting of the ice sheet. The model of the slow uplift  $U_s$  includes three parameters:  $A_s$ ,  $T_s$  and  $B_s$ :

$$U_s = \frac{2}{\pi} A_s \left[ \arctan\left(\frac{T_s}{B_s}\right) - \arctan\left(\frac{T_s - t}{B_s}\right) \right] \tag{4}$$

$A_s$  can be interpreted as half of the total isostatic uplift and  $T_s$  is the time of the maximum uplift rate correlating with the glacial retreat (15). The estimates of  $A_s$  according to (5) and  $T_s$  (ice sheet recession time) according to (16) are presented in Figure 3.

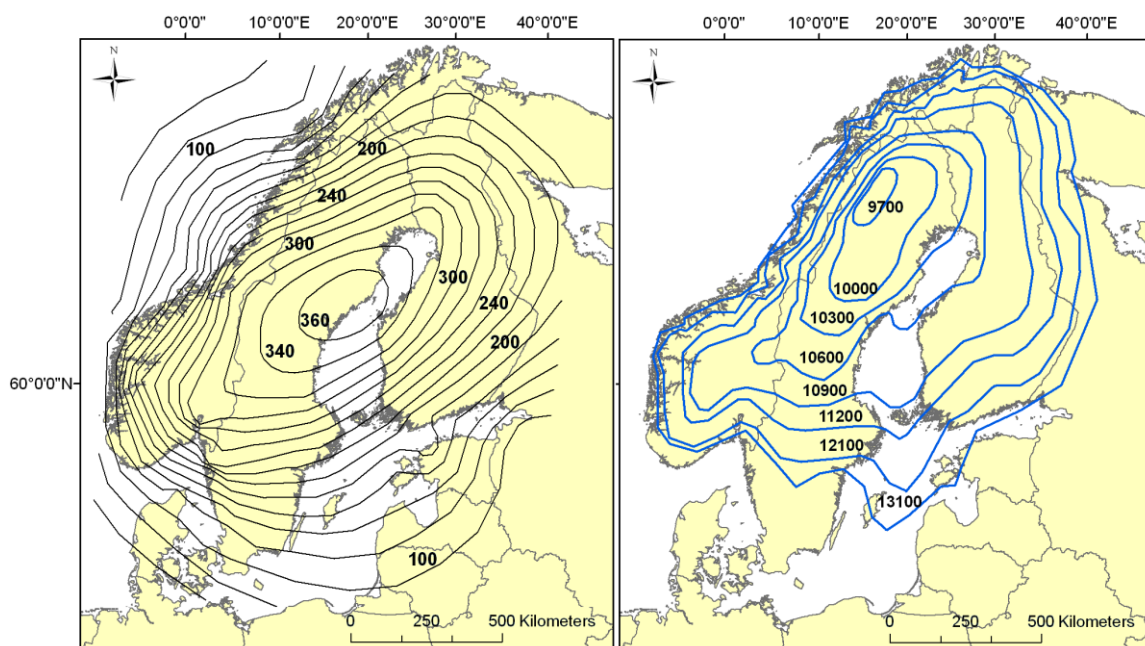


Figure 3: Left-hand side: Map of  $A_s$  (in metres) estimates in Fennoscandia (modified from (5)). Right-hand side: Map of ice recession time (in years BP) in Fennoscandia (modified from (16)).

The third parameter of slow uplift, the inertia factor  $B_s$ , has been derived using different concepts in Pässe's publications. Pässe has tested correlations between the inertia factor  $B_s$  and different mantle thickness related parameters, such as Mohorovičić discontinuity (Moho depth) and lithosphere thickness (17,18,5).

In (17), the uplift mechanism is modelled using three different parameter combinations ( $A_1, B_1, T_1$ ), ( $A_2, B_2, T_2$ ) and ( $A_3, B_3, T_3$ ). It is stated in (17) that "Resemblances exist between this (Moho) map and the map showing the variations in the values of the declining factor  $B_1$ ". The parameter values  $B_1$ - $B_3$  are presented as computation results and there is no effort to connect them to Moho depth. In (18), the fast and slow uplift mechanisms are presented. The correlation between the parameter  $B_s$  and Mohorovičić discontinuity map is expressed as:

$$B_s = 302 e^{0.067ct} \tag{5}$$

where  $ct$  is the crustal thickness of the earth. Pässe used the Moho map presented in (19) which is quite similar to the latest more detailed Moho map (20) (Figure 4).

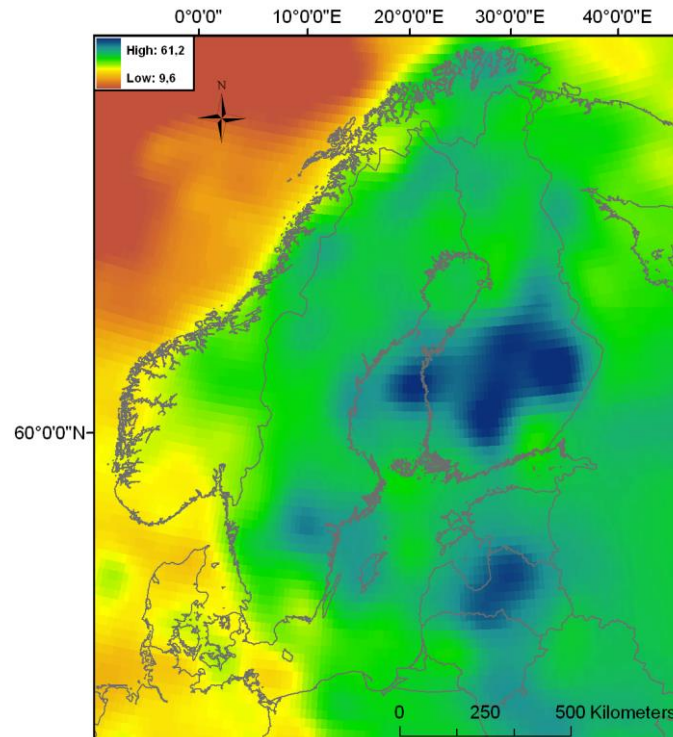


Figure 4: Map of Moho depth (in kilometres) in the Baltic Sea region (modified from (20)).

Later, Pâsse changed the reference for the  $B_s$  parameter from the Moho map to lithosphere thickness (5), where the maximum lithosphere thickness was estimated to be  $\approx 200$  km. Pâsse has taken the lithosphere thickness data from (21), where the map data has been taken from (22) and originally from (23). In these analyses, the local maximum of lithosphere thickness resides near the Gulf of Bothnia. In (24), it was estimated using the P-wave data that the local maximum of lithosphere thickness in Bothnian bay might be 160-180 km. However, (23) was criticized in (25) for the fact that the surface wave data was not able to detect the low-velocity 'asthenospheric' layer under the thickest lithosphere area in Fennoscandia. Based on the body wave data, it was suggested in (26) that the lithosphere-asthenosphere layer might be at 250 km depth. In (25), it was also found that the lithosphere-asthenosphere border might be as deep as 160 - 250 km in the Fennoscandian area using several different analysis methods (e.g., seismic, petrological and temperature). They also concluded that the lithosphere thickness is petrologically at least 240 km in eastern Finland. This supports the latest studies (27,28), where the local lithosphere thickness was found to be  $\approx 200 - 250$  km and the nearest 'local' maximum to be near Moscow, Russia. From this point of view the lithosphere thickness does not properly explain the inertia parameter  $B_s$  of Eq. (4), when the latest data are used.

Due to the dissenting opinions about the lithosphere thickness we decided to base the inertia factor  $B_s$  in our model on the Moho map of Europe as given in (20) (Figure 4). The Moho map describes the depth of the boundary between the Earth's crust and the mantle (Mohorovičić discontinuity). Based on this fact, the Moho depth can be regarded as the crustal thickness of the Earth and the inertia factor  $B_s$  can be calculated using Eq. (5).

#### Source data in model parameter estimation

Two types of input data were available for the optimization of the land uplift model parameters: one acquired from lake basins, indicating the  $^{14}\text{C}$  radiocarbon age of the sediment level where the environment changes from brackish water to fresh water indicating the lake isolation from the Baltic Sea, and the other obtained from archaeological sites of prehistoric human activity, indicating the time when the particular location definitely represented dry land.

The lake basin data set consists of 133 points. The majority of the points were obtained from (29,30,31). A complete list of the data points is found in (15). Estimation of the isolation time of the

particular locations from the Baltic Sea was based on core samples taken from the bottom of the lake basins. The layer where the freshwater algae replaced the saltwater algae was radiocarbon-dated. Also the estimate of the water level at the isolation time was determined based on observations from the surrounding landscape. The locations of the data points in this set are shown in Figure 5 (blue points).

The archaeological data set consists of 258 data points described in (32). The data set includes house and village sites, graves and ancient fireplaces. The archaeological data points represent the upper limit for the water level. The locations of the points are shown in Figure 5 (red points).

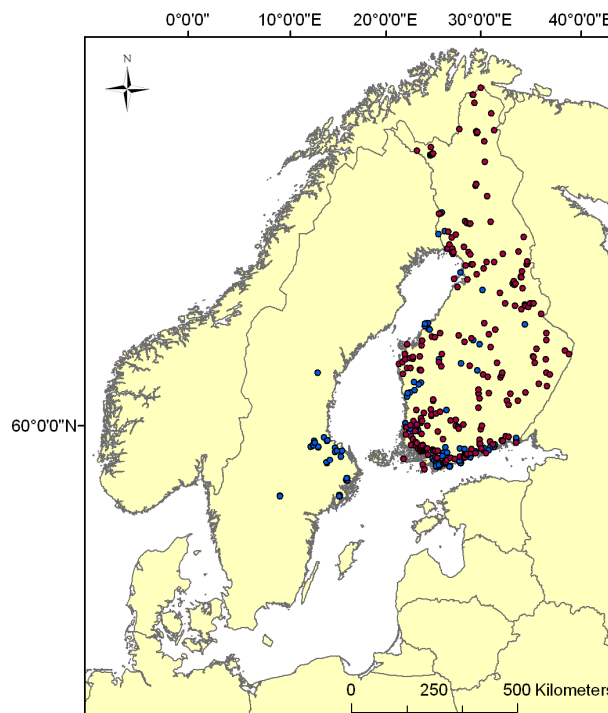


Figure 5: The lake basin data point locations (blue points) and the archaeological site data point locations (red points) in Finland and Sweden.

### Parameter refinement procedure

Both data sets involved the usage of  $^{14}\text{C}$  radiocarbon dating procedure. The “OxCal” software described in (33) was used to convert the  $^{14}\text{C}$  radiocarbon dating results into calendar years taking into account the underlying uncertainties. In Figure 6, an example of the calibration and conversion procedure of the data point from Lake Vähäjärvi in Eura is presented. Obviously, the dating procedure yields quite a complex-shaped error distribution for the age of the data point. Another source of uncertainty is the elevation value of the data points. The elevation values were obtained from the various publications describing the source data; no standard procedure could be determined for their assessment. Also, when considering the lake basin data set, various factors like erosion and previous land uplift affect the assessment of the original elevation values of lake isolation. In our modelling effort, we relied on the published elevation values taking into account their uncertainties by applying a Gaussian distribution (standard deviation of 3 m was considered to be sufficient based on the argumentation in the literature) to each elevation datum in the data sets. Monte Carlo simulation involving 1,000 realizations was then used to obtain the probabilistic estimates of the  $A_s$  and  $B_s$  parameter values of Pässe’s shore line displacement model.

The estimation of the model parameters proceeded as follows (the flow chart in Figure 7). The first task was to find the neighbouring points for the particular data point and calculate the  $A_s$  and  $B_s$  parameters. Ten nearest points were selected including the point in question and containing at least three points from the lake basin data set.

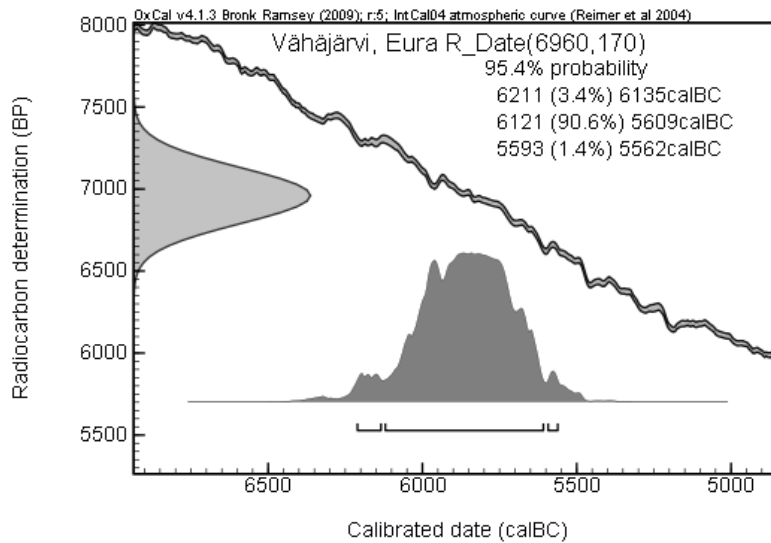


Figure 6: Screen capture from the OxCal programme. The <sup>14</sup>C age (6960) and its uncertainty (170) are the inputs. The line indicates the calibration curve, while the error distribution of the calendar age (95.4 % confidence) is shown in dark grey.

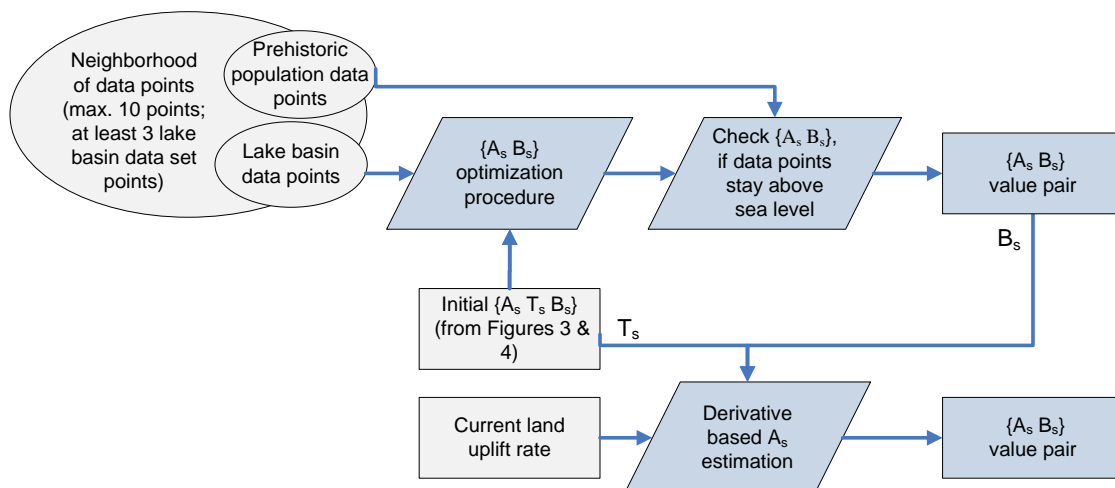


Figure 7: The flow chart of the estimation procedure.

As a starting point, an  $\{A_s B_s\}$  parameter value pair was taken based on the model and data of (5) and (20), presented in Figures 3 (left-hand side) and 4. The value of the  $T_s$  parameter was taken from (16), presented in Figure 3 (right-hand side). The optimization procedure for estimating  $A_s$  and  $B_s$  parameters was carried out using an orthogonal least squares optimization method. A region in the  $\{A_s B_s\}$  parameter space was defined, where the true parameter values were supposed to lie according to the data. This region was assigned to a cost function: the less probable the obtained parameter values were, the higher was the cost. The minimum value of the cost function was dependent on the initial parameter values of Figures 3 and 4 for the particular site, i.e., it was assumed that (5) is at least approximately right at the larger scale. An optimization procedure was then initiated and performed to produce all the parameter value pairs corresponding to the minimum values of cost functions. Curve fitting was done in the MatLab computation environment using the *fminsearch*-function, which is based on the Nelder-Mead method presented in (34).

As the prehistoric population data set presents archaeological evidence on human residence, the corresponding sites should be located above the sea level at the particular time. If the parameter values  $\{A_s B_s\}$  from the previous step indicated the opposite, the parameter values were changed step-by-step, until the resulting land uplift curve remained below the elevation obtained from the selected neighbouring points of the archaeological data set. Thus, an adjusted parameter value pair was obtained as the result. If no correction was needed and the elevation of the prehistoric

population data was higher than the sea level at the particular time as estimated by the lake basin data points, the data points of the archaeological data set were ignored.

As a comparison, another method, based on the present land uplift rate (Figure 1) and the modelling function, was used in the parameter estimation. The applied method is illustrated in (15). The  $B_s$  parameter was fixed to the value obtained at the previous step and the  $A_s$  value satisfying the current land uplift rate indicated in (6) was selected to give another parameter value pair.

The statistical estimation of parameters was performed using the Monte Carlo method (35). In this way, the resulting parameters were actually represented by probability distributions. The probability distributions were smoothed using kernel density estimation in order to get more reliable estimates for the parameter values. The calculation neighbourhood was defined for each data point so that the particular data point occurred in the centre of the neighbourhood. The resulting probabilistic parameter value pair was assigned to the location of the data point around which the neighbourhood was located.

## RESULTS

The estimation procedure was carried out using both eustatic models presented in Figure 2 (right-hand side). The results include therefore two different values for  $A_s$  and  $B_s$  parameters. An example of the distributions of 1,000 realizations of the  $A_s$  parameter obtained from the Monte Carlo simulation for the Rapajärvi data point in Rauma (lat: 61° 5.409', lon: 21° 42.453', coordinate system: WGS 84) are presented in Figure 8. The initial  $A_s$ ,  $T_s$  and  $B_s$  values were 266, 10,929 and 7,318, respectively, according to Figures 3 and 4. It can be seen that our optimization method yielded significantly lower values for this particular location. Figure 9 presents the interpolated raster images of the probabilistic  $A_s$  parameters obtained as the most probable values. The results of the  $A_s$  parameter values calculated using the derivative-based method (15) are presented in Figure 10. The raster images were interpolated using the thin plate spline interpolation method (36).

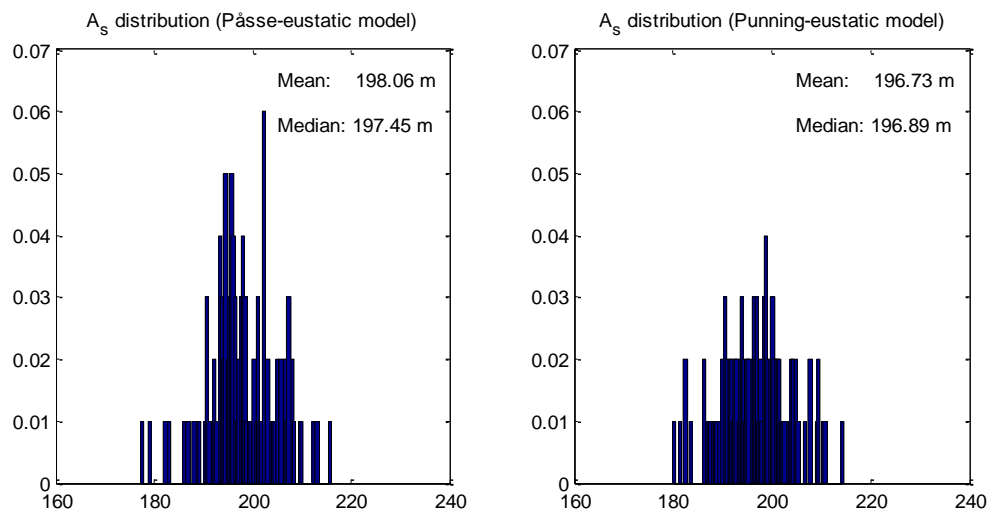


Figure 8: Simulation results of the  $A_s$  parameter for the Rapajärvi data point in Rauma. Pässe's eustatic model is used at the left panel, while the distribution at the right panel is obtained using Punning et al.'s eustatic model.

During the estimation procedure, it became clear that the download factor  $A_s$ , the ice sheet recession parameter  $T_s$  and the inertia factor  $B_s$  have a strong relationship. This can be seen from the error surface in Figure 11 (left-hand side). The error surface is shaped like a diagonal canyon without a single minimum. In the Figure, the value of the parameter  $B_s$  is fixed and the error between the model and the data is shown as a function of the values of  $A_s$  and  $T_s$ . The relationship between the slow uplift parameters seems to be almost linear. To yield a more realistic view on the model error, some *a priori* knowledge can be implied to guide the optimization procedure. For example, it is known that the ice sheet recessed within a certain time window, so this parameter cannot be arbitrary. The estimated ice recession parameter was used for guiding the estimation of the other

parameters that were assumed to be statistically Gaussian. With this *a priori* knowledge an error surface shown in the right-hand side of Figure 11 was obtained. In both cases it is clear that the error surface does not have a sharp minimum, but various different  $\{A_s, T_s\}$  parameter pairs fit the data almost equally well.

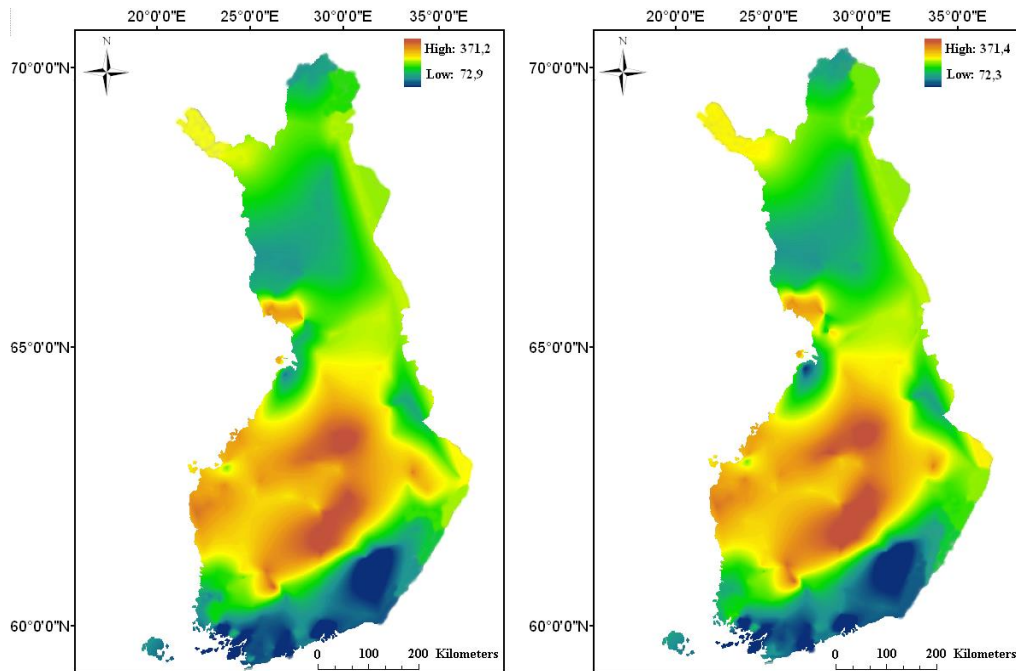


Figure 9: Maps of the  $A_s$  (in metres) parameter in the area of Finland. The left-hand side map is calculated using Pässe's eustatic model and the right-hand side map using Punning et al.'s eustatic model.

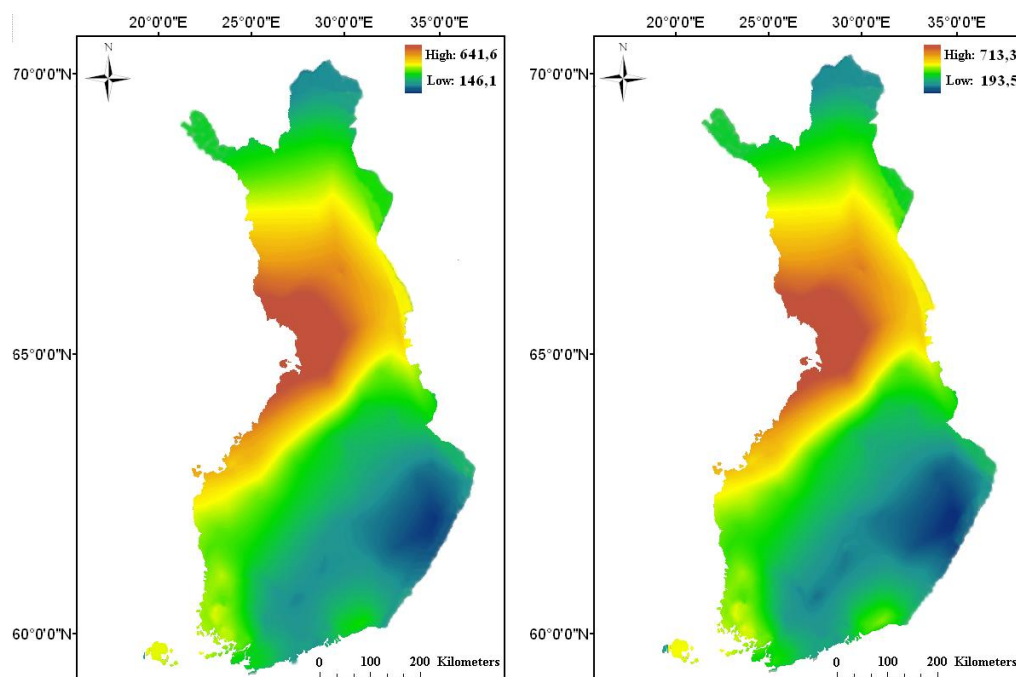


Figure 10: Maps of the  $A_s$  (in metres) parameter estimated using the derivative-based method described in (15). The left-hand side map is calculated using Pässe's eustatic model and the right-hand side map using Punning et al.'s eustatic model.

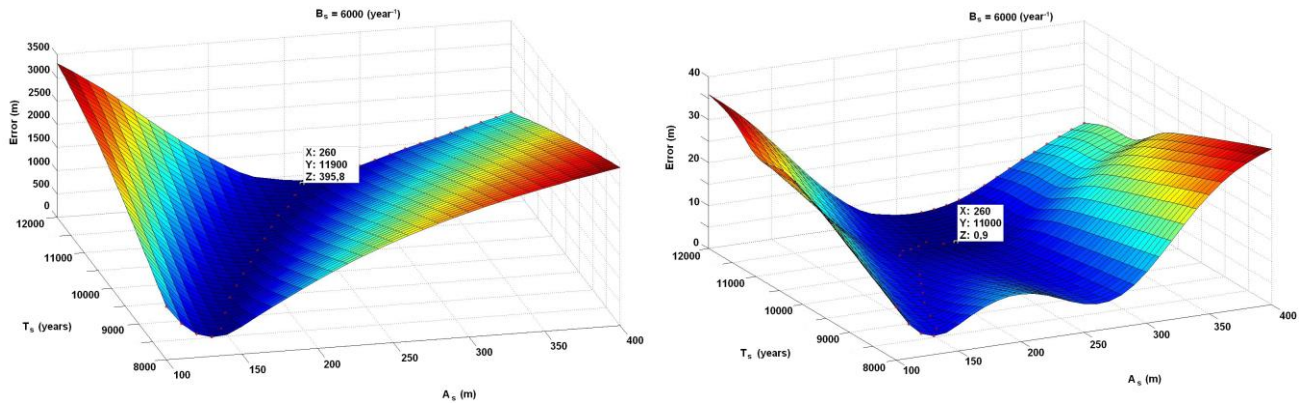


Figure 11: Left-hand side: an error surface describing the behaviour of the model error with respect to  $A_s$  and  $T_s$  with  $B_s$  fixed. Right-hand side: an error surface obtained taking into account a priori knowledge.

## CONCLUSIONS

The aim of this study was to refine the parameters of Pässe's land uplift model taking into account previously unavailable data and an alternative model of the eustatic sea level rise. Our particular interest was to find out if local deviations from the rather symmetric form of the earlier models of the land uplift can be detected based on the available data and modelling methods. When comparing our results for the  $A_s$  parameter value (Figure 9) to those presented in (5) it can be seen that the area where the largest  $A_s$  values are located (and, consequently, the average rate of land uplift has been the highest) is shifted towards Central Finland. This behaviour can be linked to the Moho depth map in Figure 4. It seems that the  $B_s$  parameter has a major influence on the estimation of the  $A_s$  parameter value. In general, the results for the  $A_s$  and  $B_s$  parameters do not differ significantly when using either Pässe's or Punning et al.'s eustatic model.

In addition to (5), it is also interesting to compare our results to those proposed in (15), where the land uplift model parameters are estimated based on the current land uplift rate using a difference-based method. The interpolated raster of the  $A_s$  parameter value, estimated using the difference-based method, is presented in Figure 10. These raster datasets follow in shape the  $A_s$  parameter distribution presented in (5), however, the values obtained here are significantly larger.

When looking at the  $A_s$  raster presented in Figure 9, sharp changes in the parameter values throughout Finland can be noticed. It is difficult to say, whether these kinds of anomalies are caused by some discrepancy in the data or reveal local variations in the land uplift rate or are caused by inadequate modelling of data. A comparison can be made with (6), where the observed land uplift rate based on three precise levellings in Finland has been presented. From the observed land uplift rate it can be noticed that there exist some local variations in land uplift in Finland. It is well known that the bedrock does not form a uniform layer but has rather a fractioned structure. Further investigation involving additional data is needed here.

Another interesting topic for future research is to employ the remotely sensed gravimetric data for refining the land uplift model. The quality of the gravimetric data is uniform within a measurement set. This kind of data is available from a significant part of the land in Finland. Gravimetric data can be used for estimating the  $B_s$  parameter value in the land uplift model either replacing the Moho or lithosphere thickness or in combination with them. Also, it would be interesting to study if the gravimetric data yields better fit with the observations and if the  $B_s$  estimations obtained using the gravimetric data and Moho or lithosphere thickness would diverge.

## REFERENCES

- 1 National Land Survey of Finland, 2012. [Laser Scanning Data](http://www.maanmittauslaitos.fi/en/maps-5). <http://www.maanmittauslaitos.fi/en/maps-5> (last date accessed: 27 May 2013)
- 2 Smith W H F & D T Sandwell, 1997. Global seafloor topography from satellite altimetry and ship depth soundings. *Science*, 277: 1957-1962
- 3 Cathles L M, 1975. *The Viscosity of the Earth's Mantle* (Princeton: Princeton University Press) 386 pp.
- 4 Lambeck K & A Purcell, 2003. [Glacial Rebound and Crustal Stress in Finland](#). Working Report 2003-10. Posiva Oy, Eurajoki, Finland. 91 pp.
- 5 Påsse T, 2001. An empirical model of glacio-isostatic movements and shore-level displacement in Fennoscandia, Report R-01-41. Swedish Nuclear Fuel and Waste Management Co., Stockholm. 59 pp.
- 6 Poutanen M, 2011. Present bedrock movements and land uplift. In: [Proceedings of a Seminar on Sea Level Displacement and Bedrock Uplift](#), 10-11 June 2010, Pori, Finland, Working Report 2011-07, edited by A Ikonen & T Lipping (Posiva Oy, Eurajoki, Finland) 25-35
- 7 Punning Y M, 1987. Holocene eustatic oscillations of the Baltic Sea level. *Journal of Coastal Research*, 3: 505-513
- 8 Fairbanks R G, 1989. A 17,000-year glacio-eustatic sea level record: influence of glacial melting rates on the Younger Dryas event and deep-ocean circulation. *Nature*, 342: 637-642
- 9 Chappell J & H Polach, 1991. Post-glacial sea-level rise from a coral record at Huon Peninsula, Papua New Guinea. *Nature*, 349: 147-149
- 10 Bard E, B Hamelin, M Arnold, L Montaggioni, G Cabioch, G Faure & F Rougerie, 1996. Deglacial sea-level record from Tahiti corals and the timing of global meltwater discharge. *Nature*, 382: 241-244
- 11 Tikkanen M & J Oksanen, 2002. [Late Weichselian and Holocene shore displacement history of the Baltic Sea in Finland](#). *Fennia*, 180: 9-20
- 12 Madsen K S, J L Høyer & C C Tscherning, 2007. Near-coastal satellite altimetry: Sea surface height variability in the North Sea-Baltic Sea area. *Geophysical Research Letters*, 34(14): L14601
- 13 Meehl G A, T F Stocker, W D Collins, P Friedlingstein, A T Gaye, J M Gregory, A Kitoh, R Knutti, J M Murphy, A Noda, S C B Raper, I G Watterson, A J Weaver & Z-C Zhao, 2007. [Global Climate Projections](#). In: [Climate Change 2007: The Physical Science Basis](#). Contribution of Working Group I to the Fourth Assessment Report of the Intergovernmental Panel on Climate Change, edited by S Solomon, D Qin, M Manning, Z Chen, M Marquis, K B Averyt, M Tignor & H L Miller (Cambridge University Press) 747-845
- 14 Brydsten L, A Engqvist, J-O Näslund & T Lindborg, 2009. [Expected extreme sea levels at Forsmark and Laxemar-Simpevarp up until year 2100](#), Technical Report TR-09-21. Swedish Nuclear Fuel and Waste Management Co. (Stockholm) 24 pp.
- 15 Vuorela A, T Penttinen & A-M Lahdenperä, 2009. [Review of Bothnian Sea shore-level displacement data and use of a GIS tool to estimate isostatic uplift](#). Working Report 2009-17. Posiva Oy, Eurajoki, Finland. 197 pp.
- 16 Sveriges geologiska undersökning (SGU), 2012. [Kartgenerator](http://maps2.sgu.se/kartgenerator/sv/maporder.html). <http://maps2.sgu.se/kartgenerator/sv/maporder.html> (last date accessed: 12 Sep 2012)
- 17 Påsse T, 1996. [A mathematical model of the shore level displacement in Fennoscandia](#). Technical Report TR-96-24. Swedish Nuclear Fuel and Waste Management Co., Stockholm, 92 pp.

- 18 Pässe T, 1997. [A mathematical model of past, present and future shore level displacement in Fennoscandia](#). Technical Report TR-97-28. Swedish Nuclear Fuel and Waste Management Co., Stockholm. 55 pp.
- 19 Kinck J J, E S Husebye & F R Larsson, 1993. The Moho depth distribution in Fennoscandia and the regional tectonic evolution from Archean to Permian times. Precambrian Research, 64: 23-51
- 20 Grad M, T Tiira & ESC Working Group, 2009. The Moho depth map of the European Plate. Geophysical Journal International, 176: 279-292
- 21 Ansorge J, D Blundell & S Mueller, 1992. Europe's lithosphere – seismic structure. In: A Continent Revealed. The European Geotraverse, edited by D Blundell, R Freeman & S Mueller (Cambridge: Cambridge University Press) 33-69
- 22 Panza G F, 1985. Lateral variations in the lithosphere in correspondence of the Southern Segment of EGT. In: Second EGT Workshop: The Southern Segment, edited by D A Galson & S Mueller (European Science Foundation, Strasbourg) 47-51
- 23 Calcagnile G, 1982. The lithosphere-asthenosphere system in Fennoscandia. Tectonophysics, 90: 19-35
- 24 Babuška V, J Plomerová & P Pajdušák, 1988. Seismologically determined deep lithosphere structure in Fennoscandia. Geologiska Foreningens Stockholm Forhandlingar, 110: 380-382
- 25 Kukkonen I T & P Peltonen, 1999. Xenolith-controlled geotherm for the central Fennoscandian Shield: implications for lithosphere-asthenosphere relations. Tectonophysics, 304: 301-315
- 26 Sacks I S, J A Snoke & E S Husebye, 1979. Lithosphere thickness beneath the Baltic Shield. Tectonophysics, 56: 101-110
- 27 Conrad C P & C Lithgow-Bertelloni, 2006. Influence of continental roots and asthenosphere on plate-mantle coupling. Geophysical Research Letters, 33
- 28 Artemieva I M & H Thybo, 2008. Deep Norden: Highlights of the lithospheric structure of Northern Europe, Iceland, and Greenland. Episodes, 31: 98-106
- 29 Eronen M, G Glückert, L Hatakka, O van de Plassche, J van der Plicht & P Rantala, 2001. Rates of Holocene isostatic uplift and relative sea-level lowering of the Baltic in SW Finland based on studies of isolation contacts. Boreas, 30: 17-30
- 30 Berglund M, 2005. The Holocene shore displacement of Gästrikland, eastern Sweden: a contribution to the knowledge of Scandinavian glacio-isostatic uplift. Journal of Quaternary Science, 20(6): 519-531
- 31 Miettinen A, H Jansson, T Alenius & G Haggrén, 2007. Late Holocene sea-level changes along the southern coast of Finland, Baltic Sea. Marine Geology, 242: 27-38
- 32 Tallavaara M, P Pesonen & M Oinonen, 2010. Prehistoric population history in eastern Fennoscandia. Journal of Archaeological Science, 37: 251-260
- 33 Oxford Radiocarbon Accelerator Unit, 2012. OxCal. <http://c14.arch.ox.ac.uk/oxcal.html> (last date accessed: 10 Sep 2012)
- 34 Nelder J & R Mead, 1965. A simplex method for function minimization. Computer Journal, 7: 308-313
- 35 Mosegaard K & M Sambridge, 2002. Monte Carlo analysis of inversion problems. Inverse Problems, 18: R29-R54
- 36 Donato G & S Belonge, 2002. Approximate Thin Plate Spline Mappings. In: Lecture Notes in Computer Science, Vol. 2352, edited by A Heyden, G Sparr, M Nielsen & P Johansen (Springer, Berlin Heidelberg) 21-31